UNIVERSITY OF TARTU

Faculty of Science and Technology

Institute of Physics

Taavi Repän

Sub-wavelength imaging with hyperbolic metamaterials

Master's thesis

Supervisors:
Sergei Zhukovsky[1]
Siim Pikker[2]

Kaitsmisele lubatud   ....

Juhendaja   ....
allkiri, kuupäev

Tartu 2014

---

[1]Technical University of Denmark
[2]University of Tartu

Contents

1 Introduction

1.1 Overview

Perhaps the most fundamental law in microscopy is the diffraction limit, discovered by Ernst Abbe in 19th century. The Abbe diffraction limit means that the imaging resolution of a microscopy is in the same order of magnitude as the wavelength. This basically limits optical microscopes from being used to image objects smaller than ~200 nm. Physicsist have of course found many ways how to cope with the diffraction limit, i.e. to obtain sub-wavelength imaging.

One way around the limit is electron microscope, which uses electron beam instead of photons. Since wavelength associated with electrons is much smaller than wavelength of visible light, electron microscopes can image even molecules (and atoms). However, this does not solve the problem completely: for many applications it is imporant not just to study the microscopic shape of the object, but its interaction with light: for example when studying small luminescent particles. Electron microscope offers very fine resolution, but no information about optical emission processes. Conventional microscopes allow to study the optical processes, but at the same time are strongly limited in resolution.

There are of course other widely used methods to obtain subwavelength imaging, scanning near-field optical microscopy (SNOM) for example. Principle of SNOM is to use small tip to scan over object and collect sub-wavelength information from near fields, which are not subject to diffraction limit. SNOM does however has its downsides, most obviously by being a scanning method: this makes hard (or impossible) to image dynamic processses.

Recent advances in nanotechnology, allowing us to build nanostructures with very fine resolution, have opened up a new avenue for working around the diffraction limit: namely *metamaterials*, nanostructures with very well tunable properties. First paper that suggested using materials with extraordinary properties was published in 1960s [1], where Veselago studied a hypothetical material, having negative refractive index. Among other features there was ability to capture and amplify evanescent near-field fields. The idea had to wait for its popularity for long time: there are no natural

materials with such properties and so the paper remained only a hypothetical.

However, in 1990s Pendry proposed an artificial structure[2, 3], which would exhibit the required negative refractive index and would allow to overcome diffraction limit. The initial proposal have their limits, but the idea of using artificial structures, metamaterials, to design artificial structures to work around the diffraction limit, begun to spread. In last 8 years structures based on hyperbolic metamaterials, *hyperlenses*, have begun to gain interest[4].

1.2 Purpose and organization of the thesis

Purpose of the thesis is to study hyperbolic metamaterials as a way for subwavelength imaging, focusing on very recent concept of dark-field hyperlens. The hyperlens strutures will be mostly studied by using full-wave simulations, provided by software package COMSOL Multiphysics.

Thesis is divided to three main parts: firstly an overview on theoretical background is given, where concepts such as metamaterials (including hyperbolic metamaterials) are discussed, along with introduction to concept of hyperlensing (i.e. use of hyperbolic metamaterials to provide sub-wavelength imaing).

Second part of the thesis consists of brief introduction to relevant numerical methods. The robustness of full-wave simulations is checked by comparing result iwth analytical solutions.

Finally, in the central, third part of the thesis a simplified version of hyperlens structure is analysed. After demonstration of tge basic properties of such structure, subwavelength imaging properties of different kinds of hyperlenses will be studied.

2 Theoretical background

2.1 Hyperbolic metamaterials

2.1.1 Metamaterials in optics

The term *metamaterial* is used in the context of artificial structures, which are engineered to have some particular properties. For example, in optics we are interested in the refractive index (or, equivalently, permittivity) of materials. In the visible spectrum the refractive index can vary roughly from near 0 (metals) to 3 (semiconductors, for example). When looking at anisotropic materials the range of materials we have is even more limited: the refractive index varies in different directions (usually) less by 10%.

If one wishes to produce more spectacular results then the limiting nature of real materials becomes an issue. Take for example transformation optics[5], which offers us a mathematical apparatus to play with the propagation of light in very creative ways. A good example of the versatility offered by transformation optics is an invisibility cloak to hide nanoscale features. But outside of purely theoretical standpoint, wishing to build a real invisibility cloak, one soon encounters the tremendous mismatch between the fantasy world of transformation optics and real world with quite limited materials. The ability to bend light at will comes at a great cost: the bending requires very strongly anisotropic materials with extraordinary properties, such as very high or negative index of refraction.

This is where metamaterials can be useful: by building different nanostructures with feature sizes much below the wavelength of the intended working regime, we can build so-called *metamaterials*. Although the artificial structure is not a homogeneous slab of material, we can say that it is effectively an artificial material, a metamaterial, which can be represented by some effective refractive index (or permittivity, as we shall do). This so called effective medium approximation works only in a certain limit, where the nanostructuring of the metamaterial is so small compared to the wavelength, that the light propagating does not sense the details of the structure itself but the average effect of the whole structure.

2.1.2 Dispersion relation for isotropic and uniaxial mediums

Before going any further, a brief introduction to dispersion relation is in order. Starting from the electromagnetic wave equation for a homogeneous isotropic medium[1]:[6]

$$\nabla^2 \mathbf{E}(\mathbf{r}, t) - \frac{\varepsilon}{c^2} \frac{\partial^2}{\partial t^2} \mathbf{E}(\mathbf{r}, t) = 0. \tag{2.1}$$

By inserting a plane wave solution, in the form of $\mathbf{E}(\mathbf{r}, t) = \mathbf{E}_0 \exp(i(\omega t - \mathbf{k} \cdot \mathbf{r}))$, into equation (2.1), we are left with the following equation:

$$\left[-\left(k_x^2 + k_y^2 + k_z^2\right) + \frac{\varepsilon \omega^2}{c^2} \right] \mathbf{E}_0 \exp(i(\omega t - \mathbf{k} \cdot \mathbf{r})) = 0. \tag{2.2}$$

To have nontrivial solutions with $\mathbf{E}_0 \neq 0$, the following condition for the wavevector components has to be satisfied:

$$k_x^2/\varepsilon + k_y^2/\varepsilon + k_z^2/\varepsilon = \omega^2/c^2 \equiv k_0^2. \tag{2.3}$$

Equation (2.3) is known as the dispersion relation and it gives a correspondence between the frequency and the allowed wavevectors for plane waves. For an isotropic medium, the dispersion relation gives well known results: plane waves propagating in the medium have a fixed wavelength ($\lambda = \frac{2\pi}{|\mathbf{k}|} = \frac{2\pi}{k_0 \sqrt{\varepsilon}}$) in any direction.

The discussion above assumed an isotropic medium, meaning that permittivity is independent of the field's polarization. This is true for many materials, but not all. For isotropic media, the constitutive relation between displacement field and electric field is $\mathbf{D} = \varepsilon \mathbf{E}$. Now, if we want to allow anisotropic mediums, permittivity is no longer a scalar, but a tensor instead: $\mathbf{D} = \boldsymbol{\varepsilon} \cdot \mathbf{E}$. We shall limit the discussion to uniaxial anisotropy, where the permittivity tensor takes the form[2]

$$\boldsymbol{\varepsilon} = \begin{pmatrix} \varepsilon & 0 & 0 \\ 0 & \varepsilon & 0 \\ 0 & 0 & \varepsilon_z \end{pmatrix}. \tag{2.4}$$

The dispersion relation (2.3) is derived for an isotropic medium, so for anisotropic mediums it does not apply directly. First of all, uniaxial mediums are birefringent, meaning that there are two kinds of propagating waves: "ordinary" and "extraordinary" wave. For ordinary waves the dispersion relation is the same as for an isotropic

---

[1]Throughout this text we are considering nonmagnetic mediums, where $\mu = 1$. Therefore μ is left out of all equations presented in the thesis.

[2]To be precise, the permittivity tensor takes diagonal form only if the coordinate axes are aligned with principal directions of the anisotropic medium.

medium, but for extraordinary waves it is the form[3][6, 7]:

$$k_x^2/\varepsilon_z + k_y^2/\varepsilon_z + k_z^2/\varepsilon = \omega^2/c^2\,. \tag{2.5}$$

From here on we shall only consider extraordinary waves, because ordinary waves behave as in an isotropic medium, making them irrelevant in the context of this thesis.

In addition to obtaining the allowed wavevectors (direction of phase velocity) from the dispersion relation, it is possible to obtain corresponding direction for group velocity as well. Normal to the isofrequency surface (in direction of increasing ω) gives the direction of group velocity[8,9]. From standpoint of physics, group velocity is much more interesting, as it gives the direction of energy flow. For an isotropic medium the isofrequency surface is sphere, for which surface normals point radially away from the surface. This corresponds to the fact that in isotropic mediums, group and phase velocities have the same direction[4]. However, for an anisotropic medium, group and phase velocities have slightly different directions, as illustrated in figure 2.1.
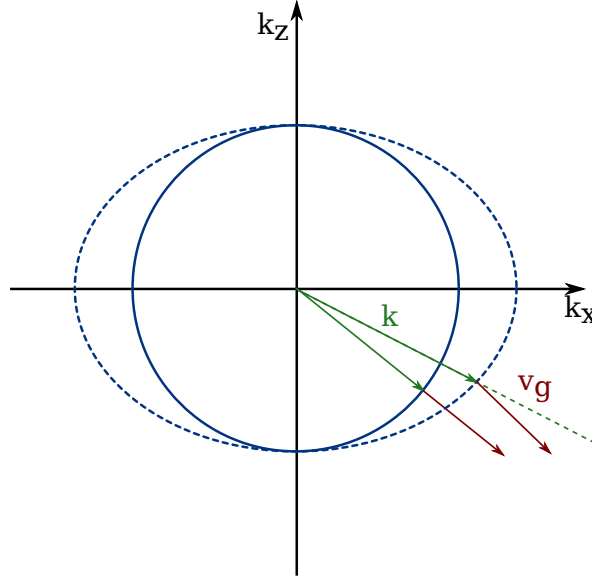

Figure 2.1: Wavevectors (green) and their corresponding group velocities (red). In this figure k_y is assumed to be zero, reducing the dispersion relation to 2D. Group velocities are normal to the isofrequency contour. For an ellipsoid the normal no longer points in a radial direction, causing the group and phase velocities to be oriented in different directions.

---

[3]The coordinate system is oriented in such way that the z-axis is taken to be along the optical axis of the uniaxial medium.

[4]Notable exception being another class of metamaterials, called negative index metamaterials. For those materials the group and phase velocities are antiparallel.

2.1.3 Hyperbolic metamaterials

For natural materials the dispersion relation (2.5) is ellipsoidal (or spherical for isotropic media). As mentioned before, metamaterials allow us to design structures with exotic properties. This means that we could design a material where the permittivity tensor components ε and ε_z have differing signs. For these structures, called *hyperbolic metamaterials* (HMM), the isofrequency surface of the dispersion relation will become hyperboloid, as shown in figure 2.2. The hyperboloid has two slightly different forms, depending on which components of permitivity tensor are negative. We shall adopt the convention as given in [10]: a dispersion with negative ε_z (one component of the tensor is negative) is called type I dispersion, whereas one caused by negative ε (two components of the tensor are negative) is type II dispersion.
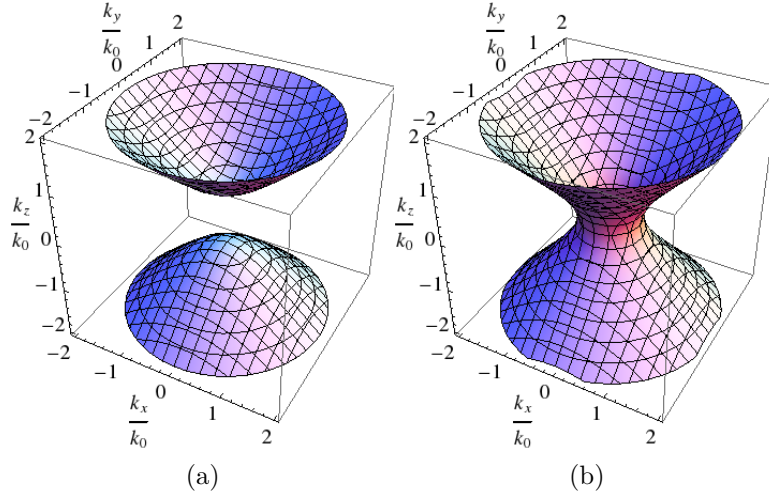

Figure 2.2: Isofrequency contours for type I (a) and type II (b) hyperbolic disperions.

They key feature of hyperbolic metamaterials, at least from subwavelength imaging standpoint, is their ability to carry waves with very large wavevectors. To illustrate this, lets consider the propagation of an arbitrary plane wave. When looking at the propagation in z direction in a homogeneous (isotropic) medium, we have the following expresison for propagation constant, according to (2.3):

$$k_z = \sqrt{\varepsilon k_0^2 - k_x^2 - k_y^2}. \tag{2.6}$$

To have propagating waves (as opposing to evanescent waves), propagation constant k_z must be real. By defining a tangential wavenumber $k^2 = k_x^2 + k_y^2$ we arrive at the following condition:

$$k^2 < \varepsilon k_0^2 \,. \tag{2.7}$$

Now, when considering hyperbolic dispersion (2.5) and using the fact that either ε or ε_z are negative, we end up with

$$k^2 > \varepsilon_z k_0^2 \,. \tag{2.8}$$

To illustrate these relations, lets consider an interface between some unspecified medium and an isotropic medium. We take the interface to be on the x-y plane, so that the normal of the surface points along z axis. In order to fulfill the necessary continuity relations of EM fields on the interface, those wavevector components that are tangential to the interface must be conserved. Supposing we have an incoming wave from the unknown medium. Without loss of generality, we set the wavevector to lie on x-z plane, giving $k_y = 0$. Now, suppose we have isotropic medium, where condition (2.7) must be fulfilled. For incoming waves for which $k_x > \sqrt{\varepsilon}k_0$ the propagation in the medium is prohibited: k_z is imaginary and the wave is evanescent in the medium. In other words, there is total internal reflection on the interface. We see that for an isotropic medium, there are waves, with large tangential wavevector, for which propagation is prohibited. In context of this thesis, these waves will be referred to as high-k waves.

Following a similar argumentation we see that for hyperbolic mediums of type I the propagation of all incoming waves is allowed. This holds true even for waves that are not propagating in the previous medium: incoming evanescent waves will become popagating inside the hyperbolic medium. For example, consider a dipole placed close to HMM, so that the dipole itself is in the air. The dipole will excite waves with wavevectors ranging from zero to infinity[5]. However, in the air, only some of these waves are propagating, the rest are evanescent. If the dipole is close enough to the HMM's surface, then many of those evanescent waves can reach the interface and will become propagating inside the hyperbolic medium.

Behavior of hyperbolic metamaterials of type II is similar, except for having a cut-off value for waves with a small tangential wavevector (low-k waves), below which propagation is not allowed.

---

[5]Dipole is delta function in coordinate space, meaning that Fourier transform of it (in wavevector space) is constant function.

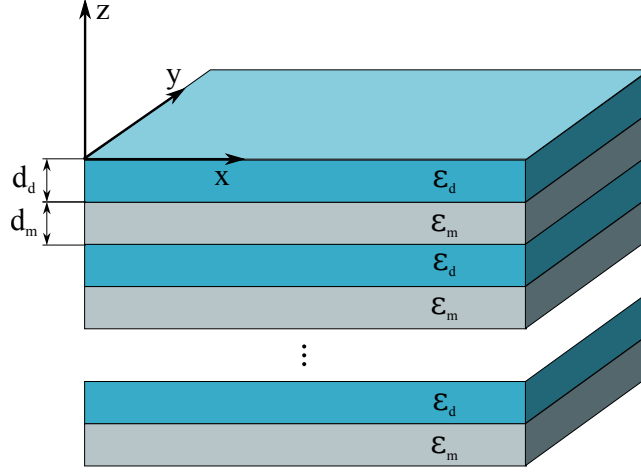## 2.1.4 Implementation of a hyperbolic metamaterial

Figure 2.3: Layered implementation of hyperbolic metamaterial. The system consists of alternating layers of metal and dielectric, with layer thicknesses d_m and d_d, respectively. Permittivites of the materials are ε_m and ε_d, respectively.

Possible implementation of a HMM is shown in figure 2.3: let us consider layered structure, consisting of thin alternating metal and dielectric layers. If the layers are sufficiently thin (compared to the wavelength), we can seek to average out the details of structure, so that its behaviour shall be describable with some effective permittivity, representing averaging of the structure. By following the procedure given in [11] we can find an effective permittivity from three parameters describing the structure: permittivites of the metal and dielectric and the composition of the structure, given by metal filling fraction defined as $\rho = \frac{d_m}{d_m + d_d}$:

$$\varepsilon = \rho \varepsilon_m + (1 - \rho) \varepsilon_d \tag{2.9}$$

$$\varepsilon_z^{-1} = \rho \varepsilon_m^{-1} + (1 - \rho) \varepsilon_d^{-1} . \tag{2.10}$$

While an ideal hyperbolic metamaterial allows propagation of waves with arbitarily high wavenumbers, this is not the case when considering realistic structures. The effective medium approach depends on the assumption that fields can be averaged over the structure, i.e. the layers are thin enough so that there are no significant effects related to individual layers. However, increasing wavevectors lead to shorter effective wavelengths. This means that at some point the effective wavelength will become comparable to the thickness of individual layers. For these waves the effective medium approximation will not hold and the structure will not behave as a

hyperbolic medium anymore. Figure 2.4 demonstrates the dispersion relation for a structure where finite thickness of layers is taken into account. For the rest of the thesis, we shall operate under effective medium approximation.
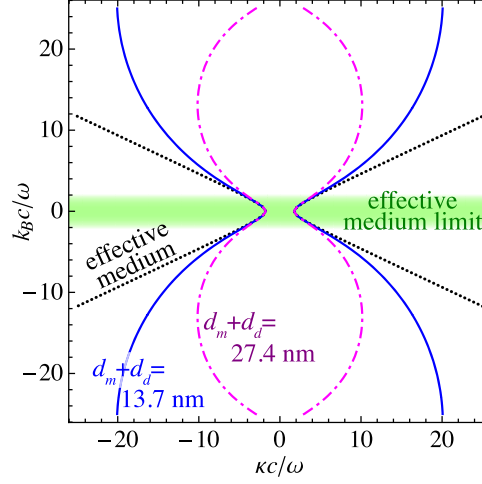

Figure 2.4: Dispersion relation for a layered structure with finite layer thickness. The dotted black line represents the dispersion relation as given by the effective medium approach. Solid blue and dashed magenta lines represent the dispersion relation when finite layer thicknesses are taken into account.
Figure reproduced from [12].

2.2 Hyperlensing

The filtering of high-k waves can be seen as the origin of the diffraction limit[13]: in conventional media the high-k waves become evanescent and will not reach the far field. The most common way to overcome this limitation is to use scanning near-field optical microscopy (SNOM), imaging the objects in the near field, so that evanescent fields can couple into the SNOM probe. The downside of this method is that it only allows imaging of one spot at the time, meaning that imaging of dynamic processes is difficult, if not impossible.

The fact that propagation of high-k waves is allowed in hyperbolic metamaterials is the basis of the idea of a hyperlens. A hyperbolic metamaterial is used to convert evanescent waves, which are carrying subwavelength information, into propagating waves inside the metamaterial. By using suitable geometry the high-k waves inside the metamaterial are transformed into low-k waves at outer interface of the hyperlens, allowing far-field imaging of subwavelength details. So far there have been two different designs proposed for this: one using cylindrically curved layered structure[14–17] and one based on an array of nanorods[18–22]. While their designs differ

drastically, the underlying working mechanism can still be described by hyperbolic dispersion[10]. This thesis shall focus on the cylindrical nanolayer design.
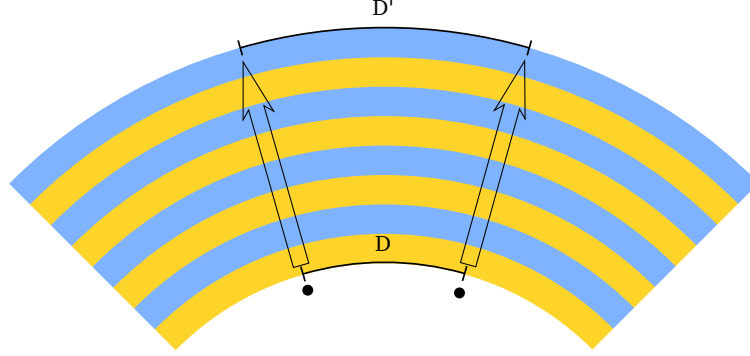

Figure 2.5: A hyperlens consisting of cylindrically curved metal-dielectric layers. Waves from two subwavelength objects (initially separated by distance D) propagate in tight beams through the hyperlens. Due to magnification from cylindrical structure, images of the objects on the outer interface are separated by distance $D' = D\frac{r_2}{r_1}$, where r_1, r_2 are inner and outer radii of the hyperlens.

The purpose of this geometry, as shown in figure 2.5, is to propagate high-k waves as a tight beam from inner surface of hyperlens to outer surface. During this propagation, owing to cylindrical symmetry, the beams will be separated, magnifing the subwavelengh features. Due to magnification the tangential wavevectors will be compressed[15], meaning that the high-k waves from subwavelength features will be transformed into low-k waves which can couple out of the hyperlens into the surrounding dielectric. Since on the outer interface the subwavelength features are now magnified above diffraction limit, they can be imaged by conventional far-field optics. The overall magnification of this kind of a structure is simply the ratio of the inner and outer radii of the cylindrical structure[23].

2.3 Concept of a dark-field hyperlens

The hyperlenses in previous section have all been designed with hyperbolic metamaterials of type I, for which all waves are allowed to propagate in. The aim of the present work is to explore a potential hyperlens based on hyperbolic metamaterials of type II. Since in this kind of HMM the propagation of low-k waves is prohibited, it would allow to design a so called *dark-field hyperlens*. The principle of this hyperlens is illustrated in figure 2.6: some subwavelength objects are illuminated with

plane wave so that scattered the high-k waves can be imaged via a hyperlens, but the original plane wave is filtered out. This allows to use a hyperlens to study, for example, objects with small scattering cross-sections, where the previously discussed bright-field hyperlenses would not offer sufficient contrast.
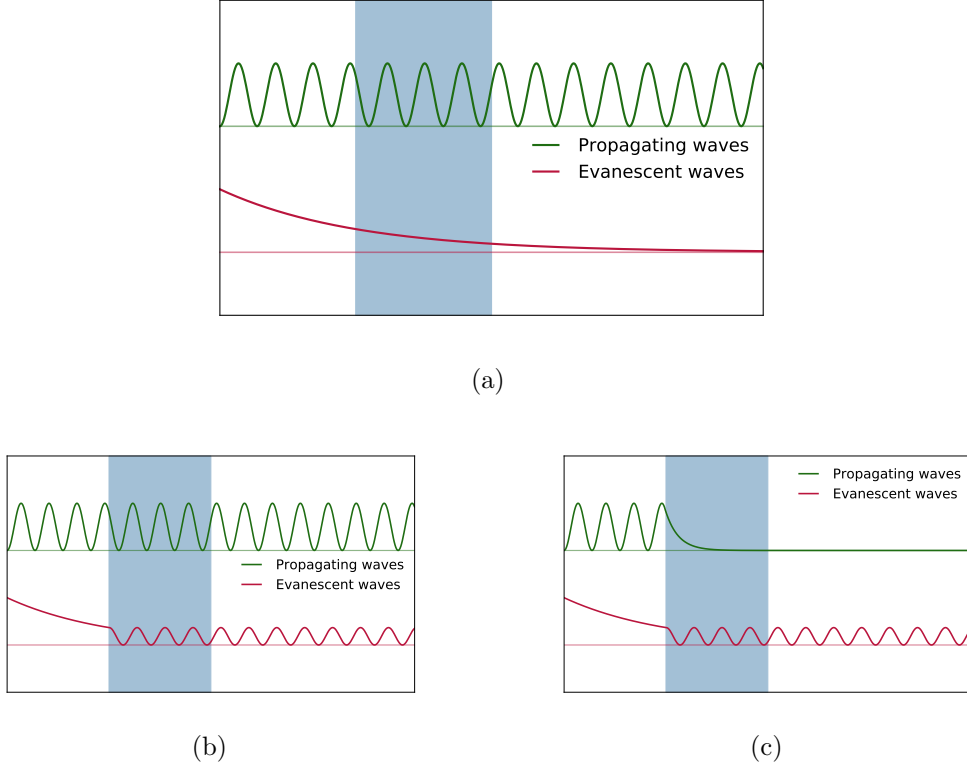

(a)

(b)

(c)

Figure 2.6: Behavior of different imaging configurations: a) conventional lens, which does not alter the nature of the waves, b) bright-field hyperlens, which turns evanescent high-k waves into propagating waves, c) dark-field hyperlens which turns evanescent high-k waves into propagating waves and at same time turns low-k waves into evanescent waves.

Using a type II hyperbolic metamaterial introduces additional constraints when designing a dark-field hyperlens. Remembering that the key feature of hyperlens geometry is the compression of tangential wavevectors for waves propagating throught the hyperlens. At same time, the type II dispersion of the HMM prohibits propagation of low-k waves through the metamaterial. This means that a compromise has to be found: potential magnification is now limited by the properties of the metamaterial. If magnification is too large, then at some point the tangential wavevector will be compressed below low-k cutoff and the fields will become evanescent. This means that the properties of the HMM have to be tuned such that it still disallows propagation of some low-k waves (facilitating dark field imaging), but on the other hand allows waves to be compresed enough for out-coupling at the outer interface.

This constraint basically requires that the medium containing the imaged object has a smaller optical density than the medium, where the far-field imaging is done. Luckily, this is not a harsh requirement considering that the measured object could be in air, but the hyperlens could be imaged through immersion oil, for example.

The idea of a dark-field hyperlens was first brought up in a paper from 2012[18], where Benisty et al. discussed an implementation of such a structure using an array of nanowires. Note that in that paper they did not use a type II HMM, but instead specially tuned excitation fields, so that they would not propagate through the hyperlens structure.

3 Towards full-wave simulations of a HMM

3.1 Numerical methods

3.1.1 Transfer-matrix method

For planar multilayer structures, such as (our implementation of) a hyperbolic meta-material, the first choice for analysis is often the transfer-matrix method (TMM). It is a simple, versatile and fully analytic method. However, it does not allow arbitrary analysis of a multilayer structure: the method deals with propagation of plane waves across a multilayer structure. Most often it is used to calculate reflection/transmission coefficients, as function of wavelength or incidence angle of light. It can also be used to find guided modes in layered structures, for designing slab waveguides, for example. However, the method lacks generality and is not usable for analyzing propagation from arbitrary sources, such as dipoles. Nevertheless, it can be used to provide a benchmark against which the full-wave solution can be verified.

Derivation of the transfer-matrix method provides no important insight in the context of the thesis, therefore only a concise overview of the key points of the method will be given. The code used for the present work is based on the formulation from [24]. The central part of the method is to, for each layer, relate the field amplitudes on the two interfaces of the layer. By assuming the fields inside a layer to be sum of a forwards and a backwards propagating wave, the field components on the interface $i + 1$ can be related to the field components on the interface i via a 2x2 matrix[1]. By multiplying the matrices corresponding to the individual layers, the final system matrix is obtained. This matrix gives relationship between the fields on the front and the back interface of the system. Reflection and transmission

---

[1] With properly aligned coordinate system for linearly polarized plane wave only three components are nonzero. Out of those components only two are independent. For example with the geometry given in [24] (layer interfaces being parallel to the y-z plane and the wavevector being on the x-y plane), for TE polarization, E_z and H_y components will be used in the method and H_x can be trivially calculated from E_z.

coefficients follow from that matrix.

3.1.2 Full-wave simulations with FEM

In range of computational methods for optics, full-wave methods take the place opposite to the analytical methods, like the transfer matrix method. Full-wave methods, such as the finite element method (FEM), solve Maxwell's equations directly, without making limiting assumptions on the problem geometry or form of the solution. Hence the term full-wave simulations, being in contrast to analytical or semi-analytical methods, which give the solution based on some eigenmodes of the problem (for example, plane waves in TMM or spherical harmonics in Mie scattering theory). This makes full-wave methods very general, allowing to study various different problems with the same method. This comes at expense of greatly increased computational complexity.

Compared to most of the other numerical methods, both theory and implementation behind finite elements methods is much more complex and involved. Therefore readily available packages are used. For present work, the COMSOL Multiphysics software packages was used, which has solvers for large array of problems, including ones for Maxwell's equations.

Basic premise of the finite element method is to divide the problem domain into a mesh of small elements. For 2D simulations the elements are usually triangles. In each of those elements homogeneous material properties are assumed and the solution (electric field in our case) is approximated as a low-order polynomial function[2] (quadratic in our case). Process of dividing the problem domain into small elements - *discretization* - also introduced new class of errors into the solution: validity of a FEM solution depends on mesh size (element size) being small enough that electric fields in each of the elements can be accurately represented by a quadratic function.

3.2 TMM calculations of HMM structure

The transfer-matrix method, being exact method for multilayer structures, can be used for preliminary studies of a hyperbolic metamaterial structure without worrying for artifacts of the finite element method, such as discretization errors. The metamaterial structure studied is shown in figure 3.1: N metal layers are interleaved with N dielectric layers of equal thickness. By varying the incidence angle of the light, waves with different transverse wavevectors are excited in the HMM. Using a

---

[2]This is strictly true only for scalar problems. For vector valued problems (such as solving Maxwell's equations) the treatment is slightly more complicated.

very high index medium ($n = 20$) allows to study propagation of high-k waves (up to $k = 20k_0$, with $k_0 = \omega/c$). Refractive index of the metal is taken to be gold at 715 nm, as given in [25].

High-index medium (n=20)

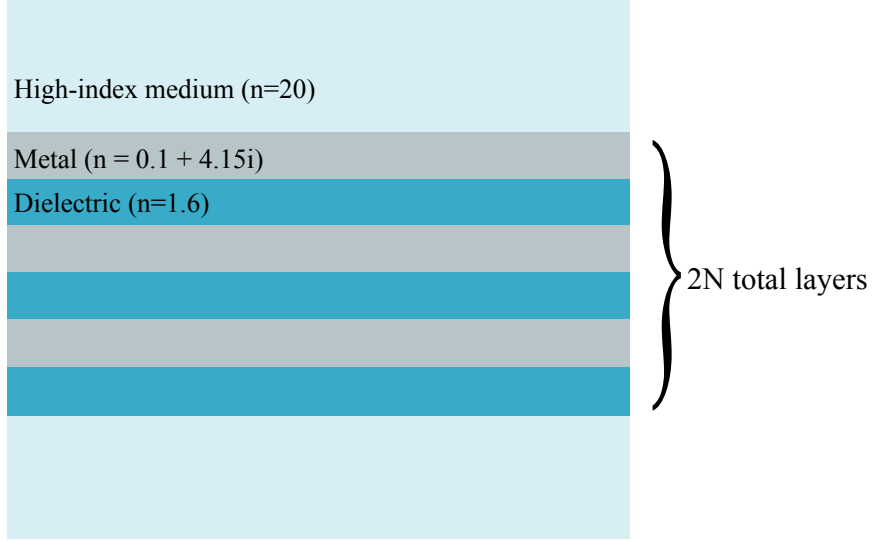Metal (n = 0.1 + 4.15i)

Dielectric (n=1.6)

2N total layers

Figure 3.1: Geometry for TMM calculations.

Using the transfer-matrix method we can calculate reflectivity curves, as function of incidence angle (i.e. transverse wavevector). The idea is to the verify behavior of the hyperbolic metamaterial structure. With conventional medium (e.g. glass) we would see reflection coefficient going to unity for high-k waves, in other terms, total internal reflection would occur. For a hyperbolic media however, we would expect those high-k waves to be able to propagate through the medium, therefore having reflection coefficient less than unity.
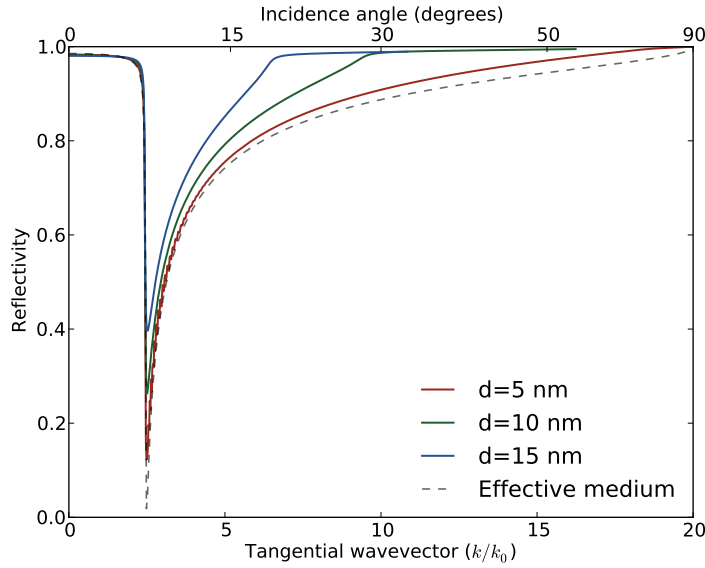
Figure 3.2: Reflectivity curves as calculated by TMM, calculated for $2N = 2 \cdot 250$ layers for varying thickness.

Results from the transfer-matrix method are displayed in figure 3.2, along with comparison with results for effective medium approximation, as given by [26]. As expected, there is a drop in reflection coefficient for some k values, suggesting propagation of those waves. We see two different regimes for strong reflections: one for low-k waves, with the cutoff point being independent of layer thickness. On other hand, for thick layers, we can also see strong reflections for high-k waves, with the cutoff point being dependent on the layer thickness.

Fact that low-k waves are being strongly reflected, suggests that the structure is behaving as a type II HMM. This is in tune with an earlier discussion on different types of hyperbolic dispersions (chapter 2.1.3), where it was established that the propagation of low-k waves is prohibited in this type of medium. Indeed, we see this in the figure: the low-k cutoff is independent of layer thickness, suggesting it being a feature of the underlying dispersion relation.

Prohibited propagation (i.e. reflection coefficent $R \sim 1$) for high-k waves, however, is not a feature of the dispersion relation: for effective medium results we see no indication of strong reflections[3]. Structures with finite layer thickness, however, display a cutoff, above which high-k waves are not propagating through the structure. As figure 3.2 shows, the cutoff point is lower as layer thicknesses increase, being indicative of breakdown of the effective medium approach, as discussed in the

---

[3]Keeping in mind that drawing any conclusions for behavior with k near $20k_0$ is somewhat complicated, given that reflection coefficient for grazing incidence approaches unity for any interface.

chapter 2.1.4.

There might be a question whether to use reflection or transmission curves to check the results. In a first glance, transmission coefficient might make more sense since we are interested in waves that are allowed to propagated through the system. Transmission coefficient, however, is strongly affected by losses in the metal. While the low-k cutoff point would still be easily observable, recognizing the high-k cutoff would be much more difficult.

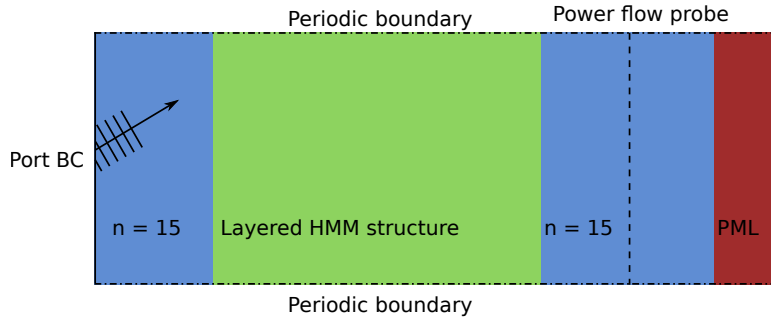## 3.3 Verifying full-wave simulations

Figure 3.3: The simulation geometry for comparing the full-wave simulation and TMM results. The port boundary condition excites plane waves from the left boundary.

Unlike analytical transfer-matrix method, the FEM is a discretized method, meaning that care has to be taken to ensure that the discretization mesh size is small enough. If the mesh is too coarse, then the finite element solution cannot accurately approximate the real result, yielding an altered solution. Having exact results from the transfer-matrix method allows to build FEM simulations for the same problem, so that that the behavior of discretization errors can be explored. The simulation geometry is shown in figure 3.3. Hyperbolic metamaterial is composed of $N = 25$ metal and dielectric layers (50 layers in total) using material properties from previous section. In addition the HMM structure, there is a spacer layer in both sides. In middle of the spacer on the right there is a power flow probe, where transmitted power is measured. Excitation is provided by a port boundary condition on the left, which also measures reflected power. In the right domain is terminated by a perfectly matched layer (PML), to absorb all the waves so they would not reflect from the simulation boundary. In transverse direction periodic boundary conditions are used.

Since discretization errors are to be expected to be more prominent when effective wavelength is small, two different scenarios were studied:

i) $n_c = 4$, serving as baseline, as no significant errors are expected

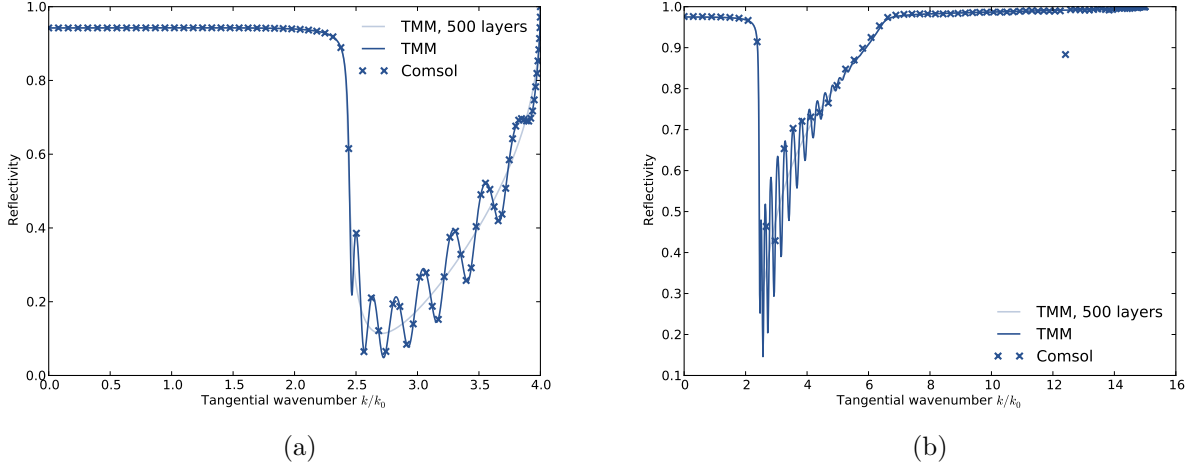ii) $n_c = 15$, for which the numerical errors should be eliminated

(a)

(b)

Figure 3.4: Reflection coefficient for $n_c = 4$ (a) and $n_c = 15$ (b) as calculated by the TMM (solid line) and FEM. The light solid line in the background shows TMM results for the HMM with $N = 250$ (e.g. 500 total layers). The layer thickness is 10 nm.

The results can be seen in figure 3.4. When compared to the results from the previous calculations (figure 3.2), there is a strong interference visible, owing to Fabry-Perot modes inside the metamaterial slab. This feature is present in both the TMM and the FEM simulations. As shown in the figure, in case of thicker slabs (having more layers) the interference fringes disappear, owing to the losses in the metal, which (given longer cavity) suppress the Fabry-Perot modes.

Overall, the FEM results are in good agreement with analytical results, especially for the low-index medium (figure 3.4a). However, when the higher-index medium is used (figure 3.4b) slight discrepancies appear in the results. In addition to that, there is anomalous dip in the reflectivity at $k \approx 13 k_0$.

To mitigate discretization errors, a smaller mesh size has to be used. At the same time, making mesh size excessively small would cause the computational complexity to become prohibitive. To better understand the role of mesh size, further simulations with varying mesh size were done with the high-index medium ($n_c = 15$). For previous calculations, maximum element size was 30 nm, which was shown to be insufficient for high-k waves.
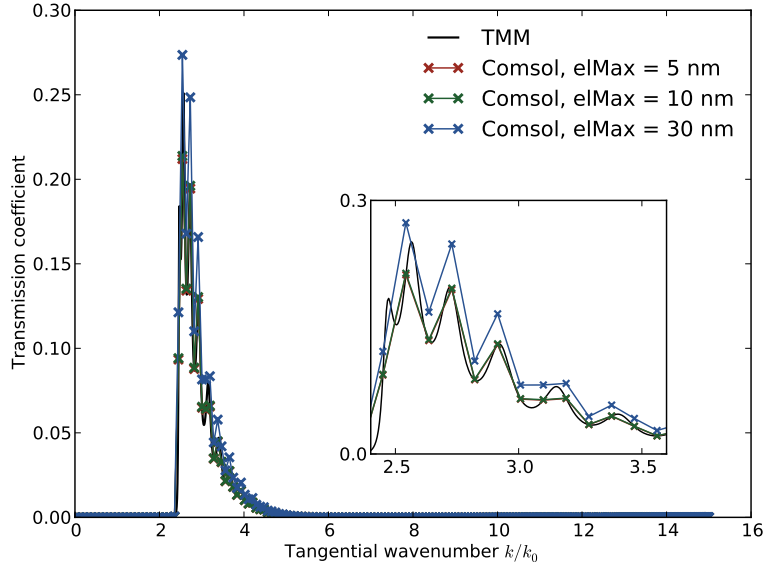
Figure 3.5: Comparison between FEM and TMM results for varing maximum element size (elMax). Transmission coefficient for layer thickness $d = 15\,\text{nm}$.

The results are shown in figure 3.5. This time transmission coefficient is plotted instead, since the numerical errors here were more prominent. As the results show, setting element size to 10 nm is already enough for results to converge to the analytical solution.
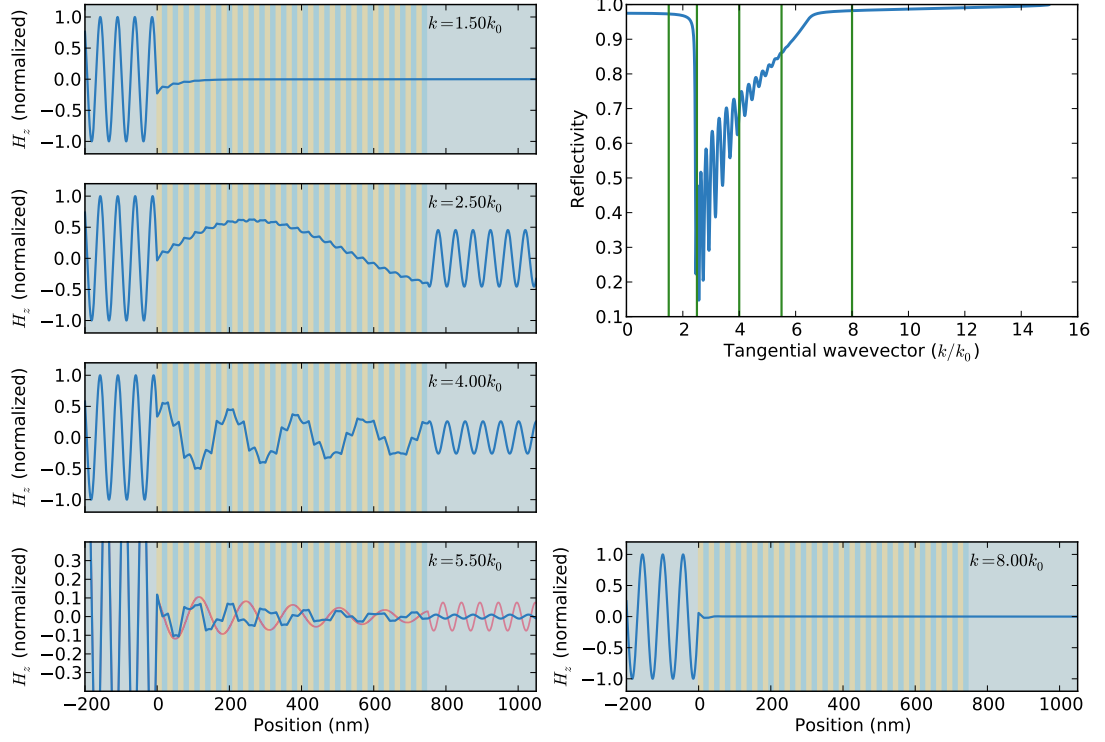
3.4 Plane wave propagation inside HMM

Figure 3.6: Demonstration of different regimes of hyperbolic metamaterial operation. Fields corresponding to different tangential wavevectors are plotted. For $k = 5.50k_0$ fields corresponding to effective medium are plotted as well, to demonstrated with the red line.

Figure 3.6 summarizes behavior of type II hyperbolic metamaterial under illumination of different incoming waves. For low-k waves the propagation is prohibited resulting in evanescent nature of the waves (figure 3.6, $k = 1.50k_0$). As the tangential wavevector is increased we enter into allowed band of high-k waves. As expected from the dispersion relation, lower k values correspond to longer effective wavelengths in the HMM (smaller k_z). With increasing tangential wavevector effective wavelength in the HMM decreases. For large k values the effective wavelength is short enough so that effective medium approach starts to break down (figure 3.6, $k = 5.50k_0$). Finally, after passing high-k cutoff the waves become evanescent again as propagation is prohibited (figure 3.6, $k = 8.00k_0$).
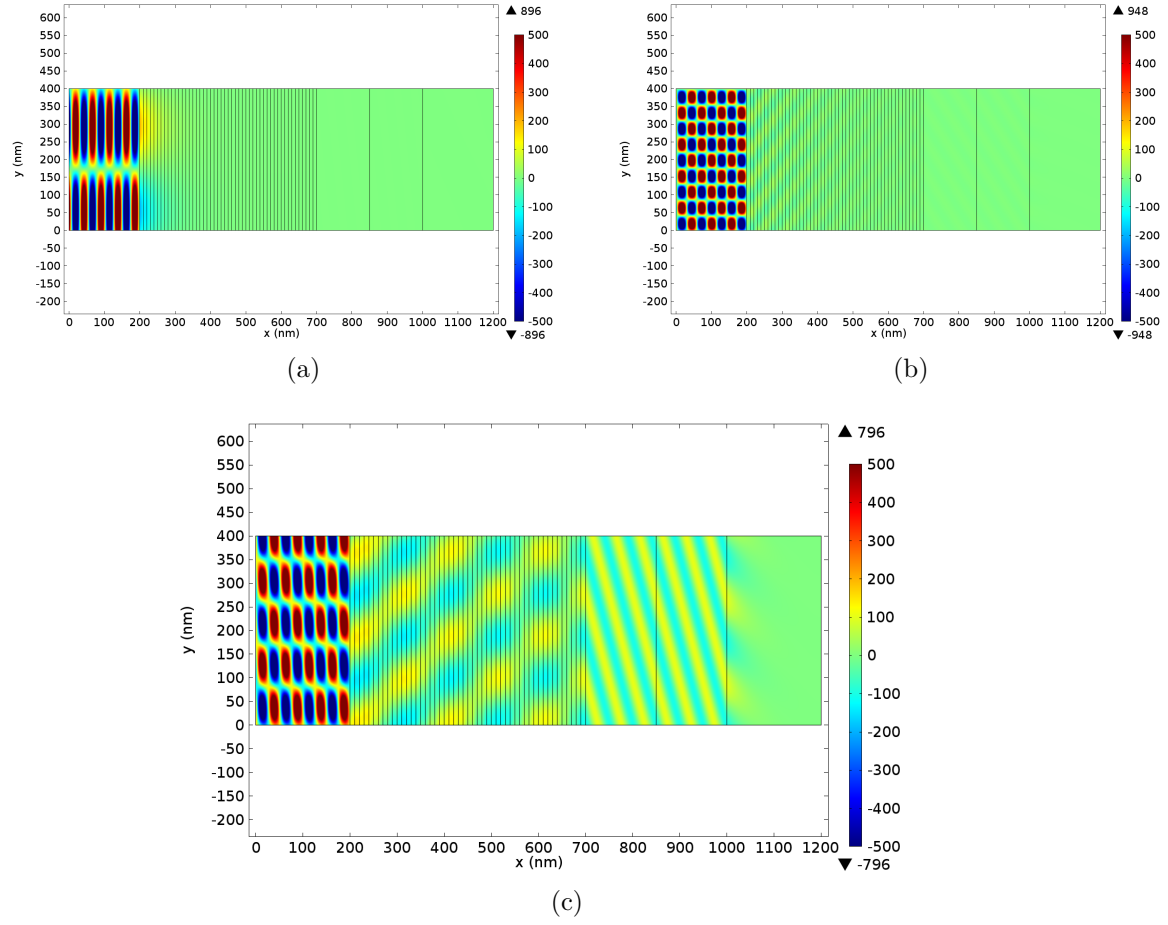
23

Figure 3.7: 2D plots of H_z fields[4], corresponding to $k = 1.5k_0$ (a), $k = 8k_0$ (b) and $k = 4k_0$ (c).

Previous results are further demonstrated in figure 3.7, where 2D full-wave simulations have performed for the key cases, demonstrating prohibited waves (figures 3.7a and 3.7b) by the low-k cutoff of HMM and by high-k breakdown of effective medium approximation, respectively. Propagation of fields through HMM is shown on 3.7c.

---

[4]In here and in all the following field plots the H_z is given in A/m.

4 Numerical study of hyperlens structure

4.1 Single dipole source

Having built methods to study and preliminary understanding of HMM structures, we shall continue towards the promise of sub-wavelength imaging with hyperbolic metamaterials. We must replace plane waves with a single dipole source, which as a delta function in space is the ultimate tool for studying sub-wavelength imaging properties of hyperbolic metamaterials.

Since a dipole source is a delta-function in physical space, its Fourier transform is composed of all wavevectors, ranging from zero to infinity. As discussed in chapter 2.1.3, most of those waves are evanescent and will not propagate away from the dipole source. As shown before, a hyperbolic metamaterial turns those evanescent high-k waves into propagating waves. By placing the dipole source close to the metamaterial, so that the evanescent waves have not yet subsided, those high-k waves could be captured and propagated in the metamaterial.
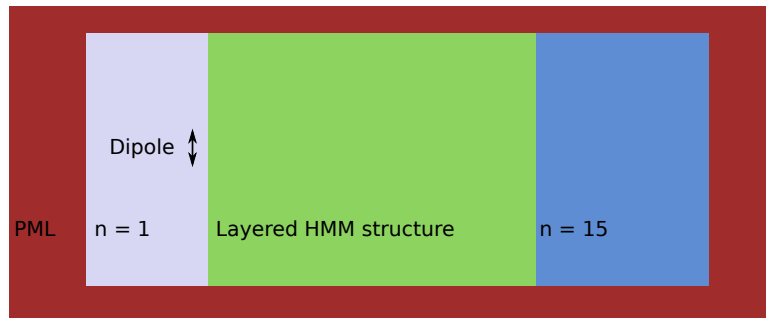

Figure 4.1: Simulation geometry for single dipole simulations.

Simulation geometry for studying system with adipole source is shown in figure 4.1. The medium containing the dipole source[1] is in the air, compared to previous simulations, where the HMM was surrounded by a high-index medium. On the other

---

[1]Since this is 2D simulation, the source is actually line dipole source, since we are forced to invariance in z-direction.

side of the metamaterial, the high-index medium is still kept for similar reasons as before: we want to be able to see the high-k waves coming out. Periodic boundary conditions are not necessary anymore and therefore a PML is used all around the simulation domain. Material properties of the HMM structure are same as in previous calculations, meaning that the structure has type II hyperbolic dispersion.
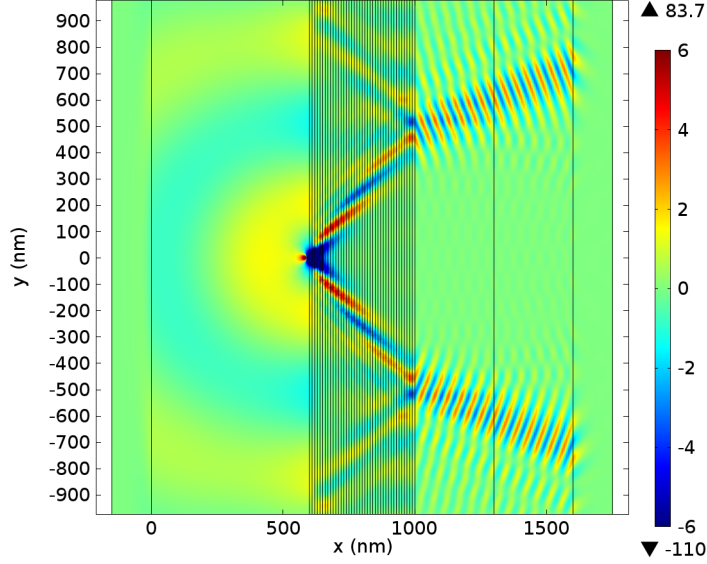

Figure 4.2: Plot of H_z fields for singe dipole simulations. The metamaterial structure consists of 50 layers in total, each layer is 10 nm thick. The dipole is placed 10 nm from the metamaterial.

Simulation results are shown in figure 4.2. Observing fields in different regions we can see that:

i) In air the familiar dipole radiation pattern is visible, as expected for isotropic dielectric.

ii) Inside the metamaterial the propagating waves form a cone, spreading the image the of dipole to a larger area. When looking closely, it is possible to see that group and phase velocities point in (almost) perpendicular directions, which is expected from a HMM.

iii) Inside high-n dielectric on the other side of the metamaterial, we see propagation of high-k waves. Also noticeable is the lack of low-k waves, which have been filtered by the type II HMM.

It is possible to demonstrate that the waves propagating through the HMM were evanescent in the air: when moving dipoles farther away from the metamaterial,

amplitude of the high-k waves will exponentially decrease, showing their evanescent nature. When measuring outcoming fields (or power) of the HMM slab, the same exponential decrease is to be expected.
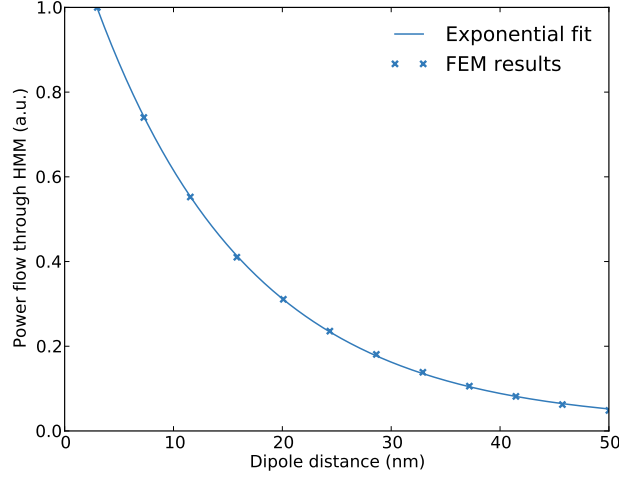

Figure 4.3: Power flow as function of dipole distance.

As shown in figure 4.3, the expected behavior is cleary seen. This substantiates previous claims that a hyperbolic metamaterial allows to capture subwavelength information from the near field.

As can be seen the fields inside the HMM travel in a cone. This causes spreading of the image on the other interface, which is generally unwanted. Firstly, this causes spreading of energy, i.e. the image of the object is fainter and this would reduce the imaging ability of the hyperlens.

Secondly this spreading causes a distortion of the image: this would be even more problematic when several dipoles (or scatterers) would be imaged. In theory the original image could still be reconstructed, but it would require some post-processing. Depending on application details, this might be feasible, but in general the spreading of the image due to "propagation cones" is unwanted and it would be beneficial to reduce this as much as possible. The regime where fields travel across the HMM without appreciable spreading is often called the "canalization regime" [27].

Recalling the equations for an effective medium (2.9-2.10) we can tune the dispersion relation by three parameters: the material parameters for metal and dielectric (tunable by choosing a material and the working wavelength) and the filling fraction of metal. It turns out that in order to make the propagation cone narrower

one would have to either reduce the metal's permittivity[2] or reduce its filling fraction. Although in reality easiest route would be to reduce filling fraction of metal, in FEM simulations it is better to change the permittivity: reducing the filling fraction would require having thinner metal layers, thereby forcing the discretization mesh to consist of smaller elements, leading to increased computational complexity. Since in simulations we are not bounded by real materials, to tune metal's permittivity for these studies a new parameter m was introduced: $\varepsilon_m = m \cdot \varepsilon_{m0}$, with ε_{m0} being the permittivity of gold at 715 nm, as used in section 3.2.
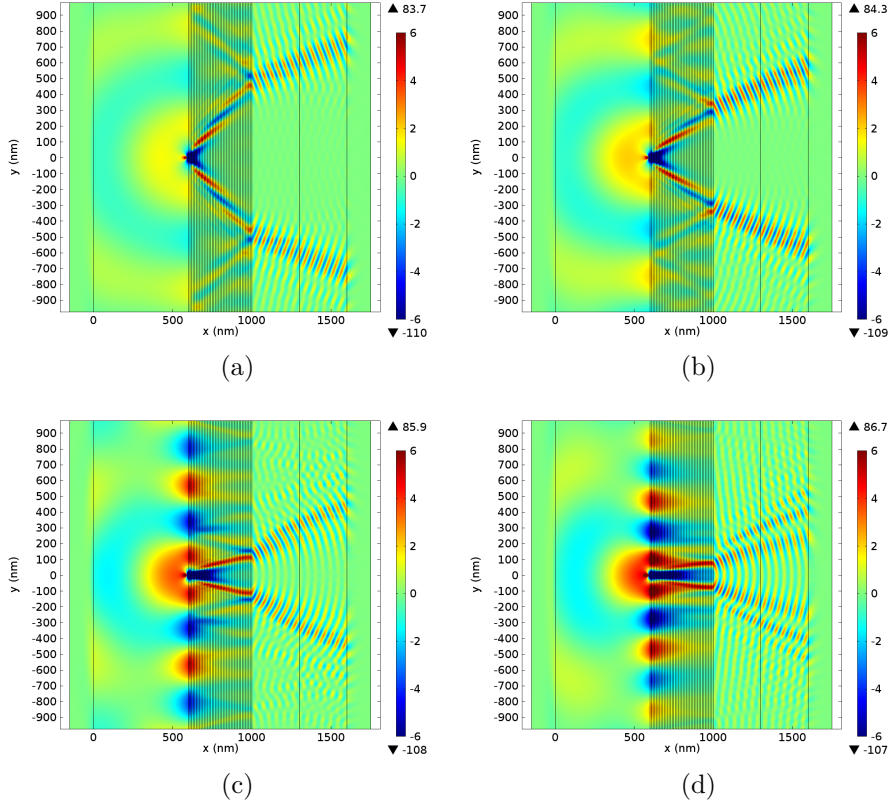

Figure 4.4: Plot of H_z fields demonstrating canalization by reducing metal permittivity): $m = 1.0$ (a), $m = 0.8$ (b), $m = 0.6$ (c) and $m = 0.55$ (d).

Figure 4.4 demonstrates the behavior of HMM as canalization regime is approached by reducing the metal's permittivity. Results clearly show that as the permittivity is reduced the propagation cone inside the HMM is made narrower. There are two side-effects visible as the canalization regime is approached: i) low-k waves start to propagate through the HMM and ii) surface plasmons appear on HMM interface. Why the surface plasmons appear is not obvious as there are multiple possible contributing factors. Since their presence is of no substantial interest in context of the

---

[2]Reduce absolute value of metal permittivity, to be exact.

hyperlens, this effect shall not be investigated here.

Propagation of low-k waves is due to the fact that although they are evanescent, their attenuation is weak enough that they can reach the other side of the metamaterial where they are allowed to propagate again. This issue can be alleviated by carefully choosing the material parameters for the hyperbolic metamaterial.

The proper hyperlens geometry would be cylindrical, but in this work discussions shall be limited to just planar HMM structures. Most of the effects (propagation of high-k waves, canalization) can still be studied with the added benefit of simpler simulations and more straightforward analysis of the results. A cylindrical hyperlens introduces additional free parameters (inner and outer radii of the structure), the choice of which would affect the results. By leaving study of magnification effects outside the scope the analysis can be simplified. As previously alluded to, a dark-field hyperlens with cylindrical design has an additional constraint to magnification by low-k cutoff. By postponing these problems, initial studies can be carried out on simplified structure, so that when later structures are to be studied, the results from simple structure could be more easily carried over. We shall refer to this structure as "poor man's hyperlens", in similar vein to the "poor man's superlens"[28].

4.2 Hyperlenses of different types and geometries

So far the discussion has been limited to only one kind of hyperbolic metamaterials: a (planar) multilayer implementation of so the called type II HMM. For comparison we also explore type I hyperbolic metamaterials and different implementations of them. In 2D treatment, the easiest way to obtain a type I HMM is to rotate the layers of a multilayer structure by 90 degrees. Of course in real world such structure would be much more complex to manufacture, but one can think of this structure as beinga 2D representation of a nanowire structure in 3D. The outcome is same: this kind of structure has hyperbolic dispersion of type I, meaning that small-k waves are allowed to propagate inside the hyperlens as well.
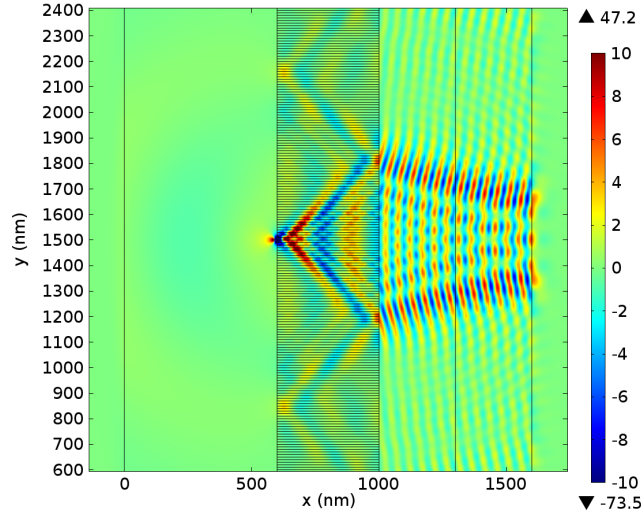
Figure 4.5: Plot of H_z fields showing the "nanorod" structure, where the layers are arranged side by side, instead of being stacked on top of each other. As before, layer thickness is 10 nm. Width of the metamaterial slab is equivalent to layered structure with total of 50 layers.

To demonstrate the properties of this "nanorod" structure, a similar simulation setup is employed as for figure 4.2, except the layered structure is replaced with a "nanorod" structure. Results are shown in figure 4.5. As expected, low-k waves propagate along with high-k waves through the metamaterial. Along with the propagation of low-k waves we see another sign of type I HMM: negative refraction for waves leaving the hyperbolic metamaterial[3].

However, it can be seen that the "nanorod" structure has rather visible artifacts. To make this more evindent we can replace the structure in the simulations with a homogeneous anisotropic material, with the permittivity taken from the effective medium approximation. This will be equivalent to having infinitely thin layers (or "nanorods" in this case).

---

[3]The demonstration of that is too lengthy to include here, but it is straightforward by following the procedure given in[8, 9].
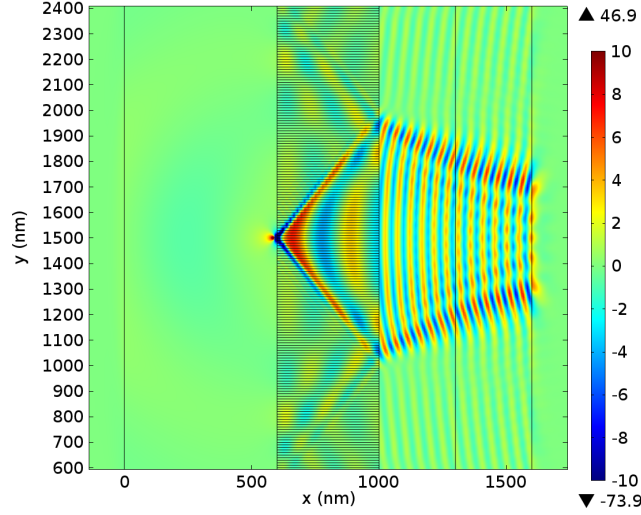
Figure 4.6: H_z plot for effective medium: the "nanorod" structure has been replaced with effective homogenous material, corresponding to a "nanorod" structure with infinitely thin layers.

Results of simulation with effective medium are shown on figure (4.6). When compared to the previous simulation with "nanorod" structure on figure (4.5), we see that a realistic structure has strong interference effects.
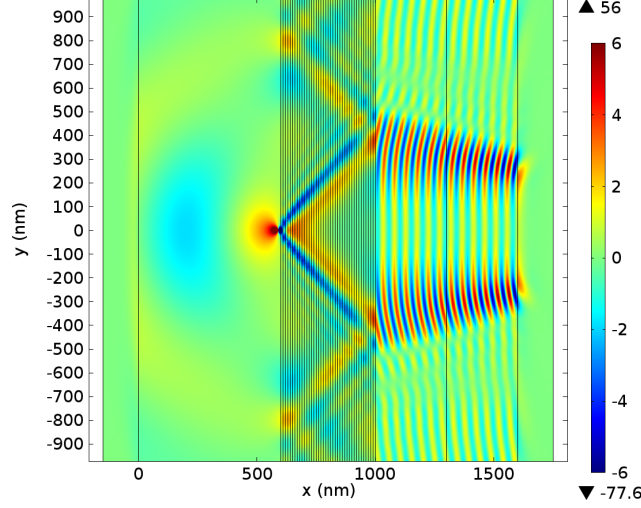

Figure 4.7: H_z plot for a type I HMM implemented using a layered structure. To get type II dispersion, metal permittivity is taken $\varepsilon_m = 0.2\varepsilon_{m0}$.

For comparison we can can also implement a type I HMM using layered structure, by choosing proper material parameters, as shown in figure 4.7. Although both structures have same layer thickness we see, that layered structure (as opposed to "nanorod" structure) approximates effective medium better[4], giving nicer fields.

---

[4]Note that figures 4.5 and 4.7 are not directly comparable, since they have different dispersion

31

Note that the interference effects present in the "nanorod" structure are not in itself really indicative of hyperlens performance. It is just that in the context of this thesis, the interence effects make the fields more complex and the figures would be harder to analyse. All the following simulations will be done using a layered structure.

Although the simulations for that are not shown here, similar conclusions can be made for type II hyperbolic materials which are implemented as "nanorod" structures.

4.3 Two dipole sources

Previous simulations demonstrated the behavior of a single dipole near an HMM structure. Those simulations demonstrated the capability of hyperbolic metamaterials to propagate subwavelength information available in high-k waves. However the subwavelength imaging itself remained a rather abstract concept. We shall now move further in that regard by having two dipoles playing the role of the subwavelength object we are imaging. As we are working with the "poor man's hyperlens" there is no magnifcation: in this geometry we just expect the images of the dipoles to be still separated after propagation through the metamaterial.
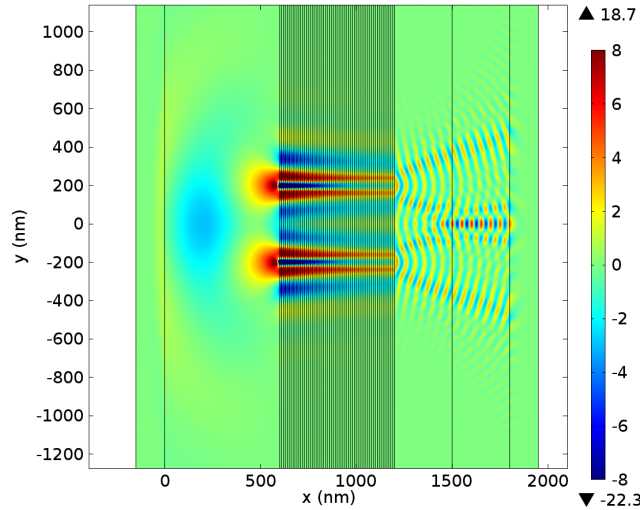

Figure 4.8: Plot of H_z fields for two dipoles. Distance between the dipoles is 400 nm, distance between the dipoles and HMM is 10 nm. For canalization metal permittivity is taken to be $\varepsilon_m = 0.5\varepsilon_{m0}$. The structure consists in total of 40 layers.

---

relation, i.e. they represent slightly different effective mediums. Nevertheless, figure 4.7 matches its corresponding effective medium calculations very well (not shown here).

The results are shown in figure 4.8: we see that the fields from single dipole propagate through the metamaterial with little divergence, i.e. in the canalization regime. The images of the two dipoles are distinguishable on the interface. This suggests that when using a proper hyperlens geometry, these dipoles could be distinguished in the far field.

To complement the previous discussions of different types of hyperbolic metamaterials in chapter 4.2, the same simulation shall be done using this type I HMM. We shall use material parameters from [16]: the metal's permittivity $\varepsilon_m = -2.4012 + 0.2488$ (gold at wavelength of 365 nm) and the permittivity of the dielectric $\varepsilon_d = 3.217$ (Al$_2$O$_3$).
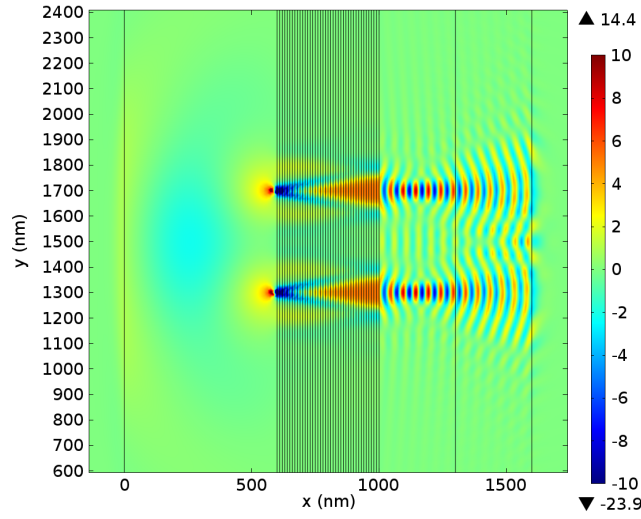

Figure 4.9: Plot of H_z fields for two dipoles. Distance between the dipoles is 400 nm, distance between the dipoles and HMM is 10 nm. The structure consists in total of 40 layers. Material parameters are chosen such to have type I dispersion.

Behavior of the type I HMM is similar, as shown in figure 4.9. The images of the two dipoles are propagated through the HMM such that they are distinguishable after the HMM. As it was alluded to in the previous chapter, a type I HMM exchibits negative refraction, leading to a slightly different image on the outer interface. Neverthelessthe two types of HMM behave identically in this kind of situation.

4.4 Conventional versus dark-field hyperlens for imaging subwavelength scatterers
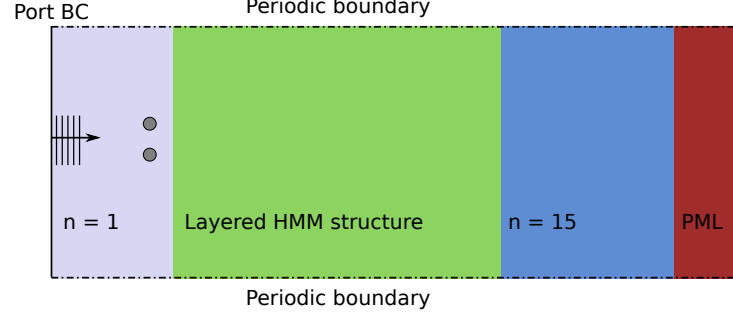

Figure 4.10: Setup for studying subwavelength scatterers.

In the previous section we considered imaging two dipoles. This models a situation where we are dealing with self-illuminating (e.g. luminescent) objects or systems where background radition will be supressed by the object itself (e.g. metal screen with subwavelength holes). Here we shall consider a different, perhaps more common, situation where we have some subwavelength scatterers illuminated by background radiation, a plane wave in our case.

Geometry of the simulations is shown in figure 4.10. The left boundary now has a port source condition, exciting a plane wave with normal incidence. Near the HMM surface are two nanorods playing the role of subwavelength objects to be imaged. In order for the effects due to scattered fields from nanorods to be stronger, the nanorods are metallic ($\varepsilon = -17.22 + 0.83i$), giving a large scattering cross section.

Note that in this case periodic boundary conditions are used. The reason for this is the fact that PML boundary condition does not work very well with a HMM structure. In theory PML should mimick the structure going to infinity but for HMM it doesn't perform very well. This caused high-k waves to originate from the PML-HMM interface and made the analysis of tge results harder. The easiest way around this was to make the boundary conditions periodic and to increase the simulation domain size so that the periodicity had no observable effects.
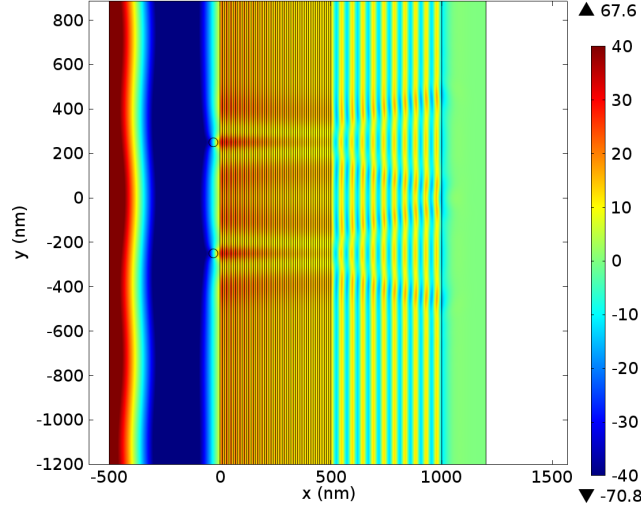
Figure 4.11: Plot of H_z fields for the bright-field HMM structure, demonstrating low contrast due to small scatterers. Structure consists of 50 layers in total, with material parameters $\varepsilon_m = -2.4012 + 0.2488$ and $\varepsilon_d = 3.217$. Scatterers are 40 nm in diameter, being separated by 500 nm from each other and by 10 nm from the metamaterial.

First we shall consider a bright-field hyperlens by using our poor man's version of a hyperlens demonstrated in [16]. Results are shown in figure 4.11. Here we see that the general behavior is similar to dipole sources in the previous chapter (figure 4.9). However we see now that there are background fields, the image contrast will be reduced.

The presence of backround fields reduces contrast and limits imaging only to objects with a large scattering cross-section (like metal particles used here). To overcome that we could use type II hyperbolic metamaterials, which, in principle, could filter out low-k waves. There are, of course, caveats: as mentioned in chapter 4.1, low-k waves are not completely filtered by the metamaterial when operating near the canalization regime. In case of lossy metals we have to take care that low-k waves die out faster than high-k waves.
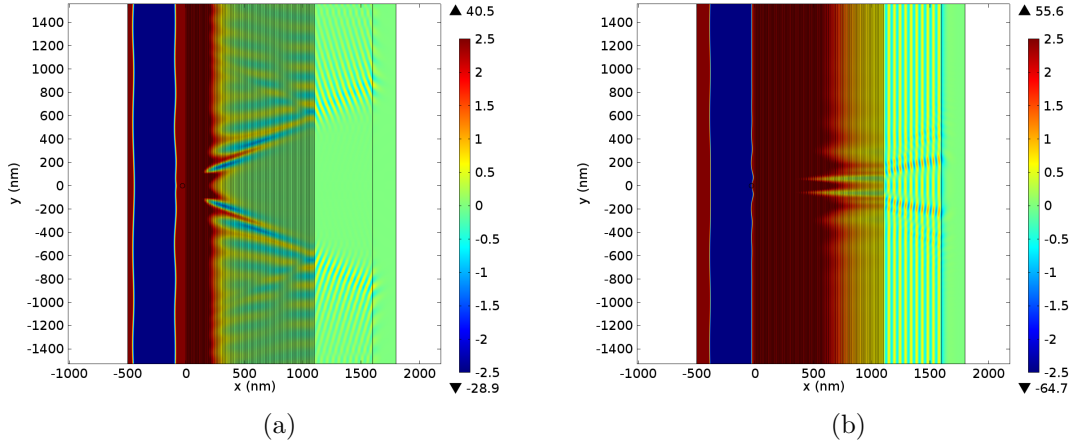
Figure 4.12: H_z plots for dark-field structure imaging single scatterer, with diameter of 40 nm, placed 10 nm from the metamaterial. Material parameters are $\varepsilon_m = -17.22 + 0.83i$ (a) and $\varepsilon_m = -4.47 + 0.30i$ (b).

This is illustrated in figure 4.12. For figure 4.12a, the material parameters were tuned such that it was operating relatively far from the canalization regime, demonstrated by large divergence of the propagation cone. For this configuration the background plane wave is filtered out. On other hand, looking at figure 4.12b, where the HMM is operating much closer to canalization regime, we see that the incoming plane wave is transmitted through the metamaterial (albeit strongly attenuated).

Compared to a bright-field hyperlens, a much thicker metamaterial slab was used, composed of $2 \cdot N = 110$ total layers (instead of 50). In addition, it was necessary to reduce losses in the metal (by artificially reducing imaginary part of permittivity). This was needed to have the low-k waves attenuated while retaining the high-k waves[5].

---

[5]The fact that low-k waves are less sensitive to losses in the metal suggests that they are still evanescent (i.e. propagation is still prohibited), but near the canalization regime their attenuation becomes weaker, comparable to high-k waves.
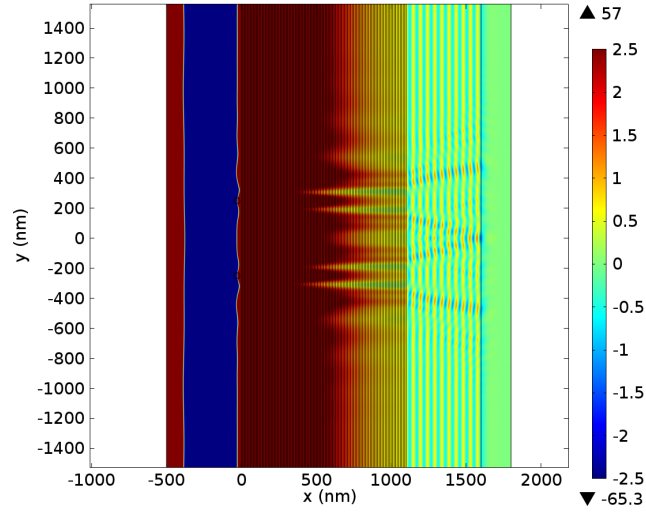
Figure 4.13: H_z plot for dark-field imaging with two scatterers, placed 500 nm apart.

Simulation of a dark-field hyperlens imaging to scatterers is shown in figure 4.13. Although the supression of low-k waves is far from ideal, the dark-field hyperlens here offers slightly better contrast (compared to bright-field hyperlens in figure 4.11). Of course there is lot of room for fine tuning the parameters. Firstly by having well-chosen parameters for the materials and secondly by making a compromise between resolution and contrast (by moving further away from the canalization regime).

5 Summary and conclusions

The main goal of this work was to study the use of hyperbolic metamaterials for subwavelength imaging, with focus on a very recent proposal of the dark-field hyperlens.

Firstly an overview and a brief introduction to topics related to metamaterials and subwavelength imaging given. This was followed by theoretical background along with implementation details of hyperbolic metamaterials. Short overview of the current research state on hyperlenses was given, along with an introduction to the dark-field hyperlens concept.

Secondly, a quick background for numerical methods, especially for the finite-element method was given. Simple properties of hyperbolic metamaterial were studied with both the analytical and the finite element method, in order to demonstrate basic principles of hyperbolic metamaterials and to study possible limitations or pitfalls of the finite element method.

The central part of the thesis was the study of a "poor man's hyperlens" structure. The term refers to the fact that we neglected study of magnification properties, allowing more straighforward analysis of fundamental properties of hyperlenses. Firstly conditions necessary for subwavelength imaging were studied, followed by an investigation of bright and dark-field hyperlenses.

Final results demonstrated that the dark-field hyperlenses can indeed provide better contrast for small scatterers. These results, combined with studies on full hyperlens structure, will be the basis of an upcoming manuscript to demonstrate a novel dark-field hyperlens based on type II hyperbolic metamaterials.

Bibliography

[1] Victor Georgievich Veselago. The electrodynamics of substances with simultaneously negative values of img align= absmiddle alt= eps/img and μ. *Physics-Uspekhi*, 10(4):509–514, 1968.

[2] JB Pendry, AJ Holden, WJ Stewart, and I Youngs. Extremely low frequency plasmons in metallic mesostructures. *Physical review letters*, 76(25):4773, 1996.

[3] John B Pendry, A J_ Holden, DJ Robbins, and WJ Stewart. Magnetism from conductors and enhanced nonlinear phenomena. *Microwave Theory and Techniques, IEEE Transactions on*, 47(11):2075–2084, 1999.

[4] Xiang Zhang and Zhaowei Liu. Superlenses to overcome the diffraction limit. *Nature materials*, 7(6):435–41, June 2008.

[5] Huanyang Chen, C T Chan, and Ping Sheng. Transformation optics and metamaterials. *Nature materials*, 9(5):387–96, May 2010.

[6] Max Born Emil Wolf. *Principles of optics (7th ed.)*. Cambridge University Press, 1999.

[7] Sukosin Thongrattanasiri. *Computational Nanooptics in Hyperbolic Metamaterials and Plasmonic Structures*. PhD thesis, Oregon State University, 2010.

[8] D. Smith and D. Schurig. Electromagnetic Wave Propagation in Media with Indefinite Permittivity and Permeability Tensors. *Physical Review Letters*, 90(7):077405, February 2003.

[9] Anan Fang, Thomas Koschny, and Costas Soukoulis. Optical anisotropic metamaterials: Negative refraction and focusing. *Physical Review B*, 79(24):245127, June 2009.

[10] Yu Guo, Ward Newman, Cristian L. Cortes, and Zubin Jacob. Applications of Hyperbolic Metamaterial Substrates. *Advances in OptoElectronics*, 2012(1):1–9, 2012.

[11] S. Anantha Ramakrishna, J. B. Pendry, M. C. K. Wiltshire, and W. J. Stewart. Imaging the near field. *Journal of Modern Optics*, 50(9):1419–1430, June 2003.

[12] SV Zhukovsky, Omar Kidwai, and JE Sipe. Physical nature of volume plasmon polaritons in hyperbolic metamaterials. *Optics express*, 21(12):14982–14987, 2013.

[13] Lukas Novotny Bert Hecht. *Principles of Nano-Optics*. Cambridge University Press, 2006.

[14] Alessandro Salandrino and Nader Engheta. Far-field subdiffraction optical microscopy using metamaterial crystals: Theory and simulations. *Physical Review B*, 74(7):075103, August 2006.

[15] Zubin Jacob, LV Alekseyev, and Evgenii Narimanov. Optical hyperlens: far-field imaging beyond the diffraction limit. *Optics express*, 14(18):8247–8256, 2006.

[16] Hyesog Lee, Zhaowei Liu, Yi Xiong, Cheng Sun, and Xiang Zhang. Development of optical hyperlens for imaging below the diffraction limit. *Optics express*, 15(24):15886–91, November 2007.

[17] Zhaowei Liu, Hyesog Lee, Yi Xiong, Cheng Sun, and Xiang Zhang. Far-field optical hyperlens magnifying sub-diffraction-limited objects. *Science (New York, N.Y.)*, 315(5819):1686, March 2007.

[18] Henri Benisty and François Goudail. Dark-field hyperlens exploiting a planar fan of tips. *Journal of the Optical Society of America B*, 29(9):2595, August 2012.

[19] Pavel Belov and Yang Hao. Subwavelength imaging at optical frequencies using a transmission device formed by a periodic layered metal-dielectric structure operating in the canalization regime. *Physical Review B*, 73(11):113110, March 2006.

[20] Atsushi Ono, Jun-ichi Kato, and Satoshi Kawata. Subwavelength optical imaging through a metallic nanorod array. *Phys. Rev. Lett.*, 95:267407, Dec 2005.

[21] G. Shvets, S. Trendafilov, J. B. Pendry, and A. Sarychev. Guiding, focusing, and sensing on the subwavelength scale using metallic wire arrays. *Phys. Rev. Lett.*, 99:053903, Aug 2007.

[22] Pekka Ikonen, Constantin Simovski, Sergei Tretyakov, Pavel Belov, and Yang Hao. Magnification of subwavelength field distributions at microwave frequencies using a wire medium slab operating in the canalization regime. *Applied Physics Letters*, 91(10):–, 2007.

[23] Dylan Lu and Zhaowei Liu. Hyperlenses and metalenses for far-field super-resolution imaging. *Nature communications*, 3:1205, January 2012.

[24] John Chilwell. Thin-films field-transfer matrix theory of planar multilayer waveguides and reflection from prism-loaded waveguides. *JOSA A*, 1(7):742–753, 1984.

[25] P. B. Johnson and R. W. Christy. Optical constants of the noble metals. *Phys. Rev. B*, 6:4370–4379, Dec 1972.

[26] Omar Kidwai, Sergei V. Zhukovsky, and J. E. Sipe. Effective-medium approach to planar multilayer hyperbolic metamaterials: Strengths and limitations. *Physical Review A*, 85(5):053842, May 2012.

[27] Pekka Ikonen, Constantin Simovski, Sergei Tretyakov, Pavel Belov, and Yang Hao. Magnification of subwavelength field distributions at microwave frequencies using a wire medium slab operating in the canalization regime. *Applied Physics Letters*, 91(10):104102, 2007.

[28] Nikolay I Zheludev. What diffraction limit? *Nature materials*, 7(6):420–422, 2008.

Summary in Estonian

HÜPERBOOLSETE METAMATERJALIDE RAKENDAMINE DIFRAKTSIOONIPIIRI ÜLETAMISEKS

Hüperboolseteks metamaterjalideks nimetatakse nanostruktuure, mida võib esimeses lähenduses käsitleda kui homogeenset keskkonda. Erinevalt looduslikekst materjalidest on metamaterjale võimalik disainida väga suures ulatuses. Hüperboolsed metamaterjalid käituvad kui ektseemselt anisotroopsed materjalid. Kõige erilisem omadus hüperboolsete metamaterjalide puhul on see, et neis saavad levida väga suure lainevektoriga lained. Selleks, et selgitada selle omaduse tähtsust tuleb meenutada, et difraktsioonipiir on oma olemuselt tingitud just kõrge lainevektoriga lainete välja filtreerimisest: harilikes keskkondades ei saa sellised lained levida ning nad eksisteerivad vaid objekti lähedal lähiväljas. Kuna nende, suure lainevektoriga lainete levik hüperboolses metamaterjalis on lubatud, siis see tähendab, et seda saab rakendada difraktsioonipiiri ületamiseks. Sellist struktuuri, mille abil seda on võimalik teha nimetatakse hüperläätseks.

Selle töö eesmärgiks on uurida üht konkreetset hüperläätse tüüp: pimevälja hüperläätse. Pimevälja hüperläätse idee pakuti esimest korda välja 2012. aastal. Selle töö eesmärgiks oli uurida sellise hüperläätse disaini, kasutades ???? hüperboolset metamaterjali.

Alustuseks anti töös ülevaade hüperboolsete metamaterjalide omadustest ning taustats. Lisaks demonstreeriti hüperboolse metamaterjali praktilist realisatsiooni, kihilise nanostruktuuri näol. Anti põgus ülevaade praeguseks välja pakutud hüperläätsede disainidest, sealhulgas uudsest pimevälja hüperläätse omast.

Edasi tutvustati töös kasutatud numbrilisi meetodeid: ülekandemaatriksi meetodit (*transfer-matrix method*) ja lõplike elementide meetodit (*finite-element method*). Lõplike elementide simulatsioone kontrolliti analüütiliste tulemustega ning sellega veenduti meetodi töökindluses. Demonstreeriti ka lihtsamaid hüperboolsete metamaterjalide omadusi.

Töö peamine osa keskendus hüperläätse uurimisele, täpsemalt "vaese mehe hüperläätsele" (*poor man's hyperlens*), mis viitab sellele, et ei uuritud täielikku hüperläätse

disaini, vaid piirduti lihtsama struktuuriga. Selle lihtsama struktuuri puhul jäetakse uurimata hüperläätse suurendus ning sellega seodnuvad efektid. See lihtsustas tulemuste analüüsimist ning järelduste tegemist.

Töös võrreldi tavalist, ehk helevälja hüperläätse, tumevälja hüperläätsega. Võrdluste käigus selgus, et väikeste hajutajate uurimisel on tumevälja hüperläätsega võimalik saavutada paremat pildi kontrasti, kuna taustakiirgus filtreeritakse välja.

Töö tulemuste põhjal on valmimas teadusartikkel, kus tutvustatakse uut liiki tumevälja hüperläätse ning selle omadusi.

Non-exclusive license to reproduce thesis and make thesis public

I, Taavi Repän (date of birth: 08.04.1990),

1. herewith grant the University of Tartu a free permit (non-exclusive license) to:

> **1.1** reproduce, for the purpose of preservation and making available to the public, including for addition to the DSpace digital archives until expiry of the term of validity of the copyright, and

> **1.2** make available to the public via the web environment of the University of Tartu, including via the DSpace digital archives until expiry of the term of validity of the copyright,

Sub-wavelength imaging with hyperbolic metamaterials,

supervised by Sergei Zhukovsky and Siim Pikker,

2. I am aware of the fact that the author retains these rights.

3. I certify that granting the non-exclusive license does not infringe the intellectual property rights or rights arising from the Personal Data Protection Act.

Tartu, 02.06.2014